Optical Materials 36 (2014) 712–716

Contents lists available at ScienceDirect

Optical Materials

journal homepage: www.elsevier.com/locate/optmat

Role of defects concentration on optical and carbon dioxide gas sensing properties of Sb_2O_3/graphene composites

K.R. Nemade, S.A. Waghuley *

Department of Physics, Sant Gadge Baba Amravati University, Amravati 444 602, India

ARTICLE INFO

Article history:
Received 4 September 2013
Received in revised form 15 November 2013
Accepted 21 November 2013
Available online 8 December 2013

Keywords:
Graphene
Optical properties
Gas sensing

ABSTRACT

Sb_2O_3 quantum dots (QDs) anchored graphene composites were prepared by *in situ* chemical route, followed by the subsequent annealing. The chemiresistors in the form of thin film fabricated using composites powder exhibit considerable response to carbon dioxide (CO_2) gas. The resulting samples were characterized by X-ray diffraction and electron microscopy for structural and morphological analysis. Ultraviolet–visible spectroscopy was performed to the quantum confinement effect in Sb_2O_3 quantum dots. Fluorescence spectroscopy was employed to study the dependence of gas sensing response on optical properties and defects density. The chemiresistors shows almost linear response up to 50 ppm CO_2. Among those chemiresistors, 1.6 wt% graphene chemiresistor shows the best response. The response and recovery times to 50 ppm CO_2 for 1.6 wt% graphene chemiresistor at room temperature are 16 and 22 s, respectively.

1. Introduction

Carbon dioxide (CO_2) is an essential part of earth atmosphere, it continuously being exchanged between the atmosphere, sea and soil surface. Ocean absorbing CO_2 from the atmosphere, this result in ocean acidification and subsequently cause to climate change [1]. Moreover, CO_2 is green house gas. Graphene sheets decorated with metal oxide quantum dots might result in the good gas sensing properties [2–4]. Also, graphene surface anchored metal oxide nanoparticles can provide greater usefulness in gas adsorption and sensing processes [5–7].

With this mind, we developed efficient chemiresistors for an effective monitoring of CO_2. In this regards, present work comprises a bold attempt to develop a chemiresistor based upon unattempted sensing material graphene/Sb_2O_3 composite. During literature survey, there are few reports related to the graphene/Sb_2O_3 composite and it is for the first time, we explored graphene/Sb_2O_3quantum dots composites as a CO_2 sensing material. Our experiment clearly focused onto reduce the operation cost by operating chemiresistors at low temperatures with effective sensing of test gas. Some interesting accomplishments are also reported.

2. Experimental

In this work, we adopted a convenient *in situ* method to prepare Sb_2O_3 quantum dots (QDs) anchored graphene composites. The graphene used in this work was prepared by a previously reported method [8]. The preparation of Sb_2O_3 QDs anchored graphene composites could be divided into two steps: First, in two separate beakers, $SbCl_5$ and NaOH dissolved in deionized water of resistivity not less than 18.2 MΩ/cm with molar ratio 1:5. The solution was put in an ultrasonic bath for 8 h. Second, graphene was mixed in solution placed in oven to dry at 100 °C. The dried products were sintered in a quartz tube at 200 °C for 8 h under a nitrogen atmosphere. In this way, four samples were prepared by varying wt% of graphene from 0.4 to 1.6 wt%.

The X-ray diffraction patterns were acquired on Rigaku (Miniflex (II)) diffractometer with Cu Kα radiation in the range from 10° to 70°. The morphology of sample was analysed through FE-SEM and TEM by using JEOL JSM-7500F and (JEOL-1200ex), respectively. Raman spectroscopy (RFS 27; Bruker; Raman spectrometer) was employed to illustrate the interaction between pristine graphene and Sb_2O_3 QDs using a Nd:YAG laser excitation source of wavelength 514 nm. The UV–vis analysis performed on Perkin Elmer UV spectrophotometer in the range 205–705 nm. The fluorescence analysis was performed on FL Spectrophotometer (Model: HITACHI, F-7000).

The chemiresistors in the form of thin film were prepared by screen-printing technique on glass substrate of size 25 mm × 25 mm by using temporary binder, composed of butyl carbitol and ethyl cellulose. For sensing measurements, ohmic contact was achieved by using highly conducting silver paint deposited on adjacent sides of the chemiresistor and heating the chemiresistors at 100 °C for 30 min in argon atmosphere. The average thickness of chemiresistors was about 6 μm, measured by Digimatic Outside Micrometer (Series-293, Japan). In order to

* Corresponding author. Tel.: +91 9423124882; fax: +91 07212662135.
E-mail address: sandeepwaghuley@sgbau.ac.in (S.A. Waghuley).

0925-3467/$ - see front matter © 2013 Elsevier B.V. All rights reserved.
http://dx.doi.org/10.1016/j.optmat.2013.11.024

investigate gas sensing properties, the gas sensor unit was specially designed. Dry air (H_2O lower than 2 ppm) was used as carrier gas. The sensing response is defined as given below [9]:

$$S = \frac{\Delta R}{R_a} = \frac{|R_g - R_a|}{R_a} \quad (1)$$

where Ra and Rg are the resistance of chemiresistor in air and gas, respectively.

3. Results and discussion

Fig. 1 shows the typical X-ray diffraction (XRD) pattern of the graphene and as-prepared Sb_2O_3/graphene composite, clearly suggestive of the formation of Sb_2O_3 quantum dots with very small size reflects from highly broadened diffraction peaks. These results are also confirmed by FE-SEM and TEM as described later. No sharp peaks corresponding to Sb_2O_3 QDs are observed in the powder pattern, which might attribute to the appearance of broad characteristics peaks of graphene that is (002) and (100) [10]. Hence, individuals' peaks of Sb_2O_3 QDs suppressed under the characteristics peaks of graphene. This statement is well supported by selected area electron diffraction analysis. The average crystallite size for composites was estimated by using Scherrer's formula, which ranges between 4 and 8 nm.

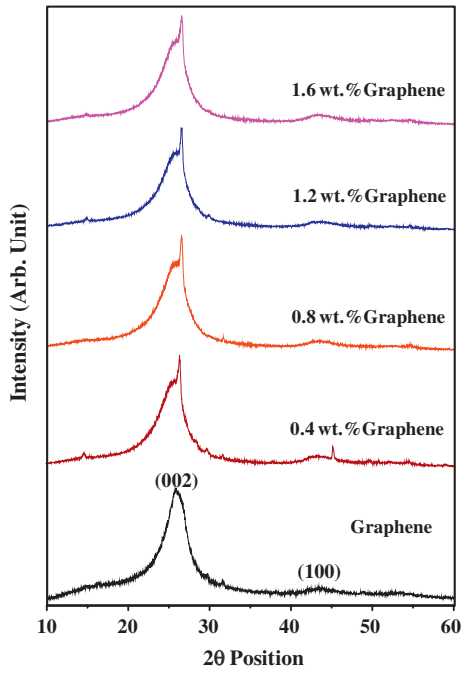

Fig. 1. XRD patterns of graphene and graphene/Sb_2O_3 QDs composites.

The morphology and structural features of as-synthesized 1.6 wt% graphene/Sb_2O_3 QDs composite were elucidated by FE-SEM and TEM, as it is optimized sample discussed later. Fig. 2(a) shows the FE-SEM micrograph of 1.6 wt% graphene/Sb_2O_3 QDs composite, indicates that Sb_2O_3 QDs are entirely anchored on graphene sheets. The small amount of agglomeration is present in sample. Fig. 2(b) shows the TEM image, reflects that large amount of Sb_2O_3 QDs were distributed on the graphene sheets.

As XRD analysis unable to specify clearly presence of Sb_2O_3 QDs, selected area electron diffraction (SAED) analysis was performed to support the presence of Sb_2O_3 QDs. The SAED image is presented in inset of Fig. 2(b). The several broad diffracting rings could be identified in the diffraction pattern. The rings observed in diffraction pattern attributed to presence of Sb_2O_3 QDs, because pristine graphene shows only hexagonal symmetry with clear six spot patterns [11]. This stipulates that white platelets observed in FE-SEM image are Sb_2O_3 QDs.

Fig. 3 presents UV–vis spectrum of pristine graphene and graphene/Sb_2O_3 QDs composites. The UV–vis spectrum of graphene shows sharp absorption at 268 nm, whereas spectrum of composites exhibits absorption around the 206–210 nm. The blue shift is observed in case of composites. This shifting towards the lower wavelength attributed to the synergetic effect of graphene and Sb_2O_3 QDs. This confirmed the existence of strong quantum confinement, which is fundamental characteristic of quantum dots [12].

Fig. 4 displays fluorescence spectrum of as-obtained composites and pristine graphene, recorded in the range 315–715 nm under excitation. The fluorescence spectrum shows that composite samples possess broad emission in ultraviolet region, whereas in visible region shows the nearly flat emission.

To establish the interaction between pristine graphene and Sb_2O_3 QDs Raman spectroscopy was performed. Fig. 5 depicts the Raman spectra of graphene and 1.6 wt% graphene/Sb_2O_3 QDs composite recorded at room temperature. The intensities of almost all bands shown in the Raman spectrum were appreciably affected. Along with these bands, the D band is strappingly affected. This may be due to Sb_2O_3 QDs affect the one-phonon lattice vibration process. Furthermore, this demonstrate that Sb_2O_3 QDs act as active sensing sites by damaging to the graphene sheets, which may generates vacancies or dangling bonds on graphene surface. The X-ray photoelectron spectroscopy (XPS) measurements could

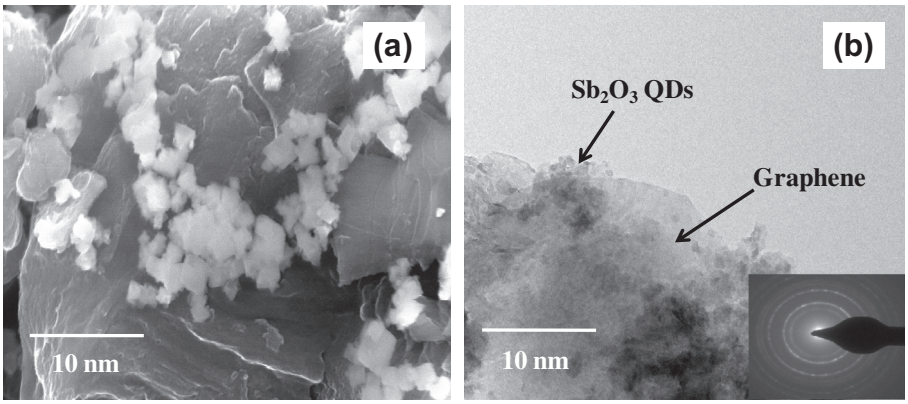

Fig. 2. (a) FE-SEM and (b) TEM image of 1.6 wt% graphene/Sb_2O_3 QDs composite from the edge-side view. Inset shows SAED image.

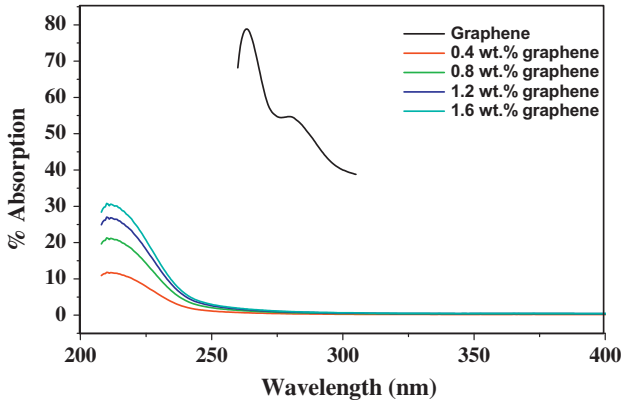

Fig. 3. UV–vis spectrum of graphene and graphene/Sb_2O_3 QDs composites.

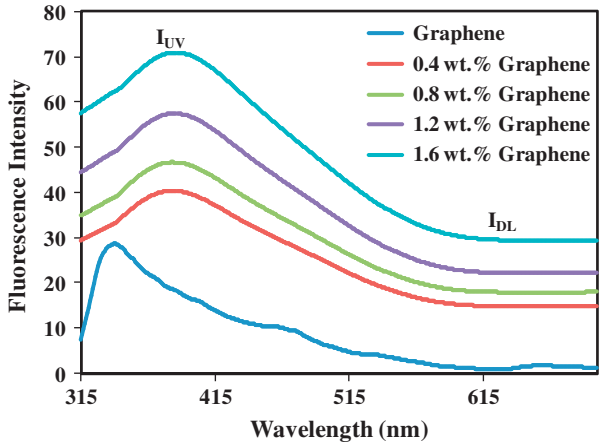

Fig. 4. Fluorescence spectrum of graphene and graphene/Sb_2O_3 QDs composites.

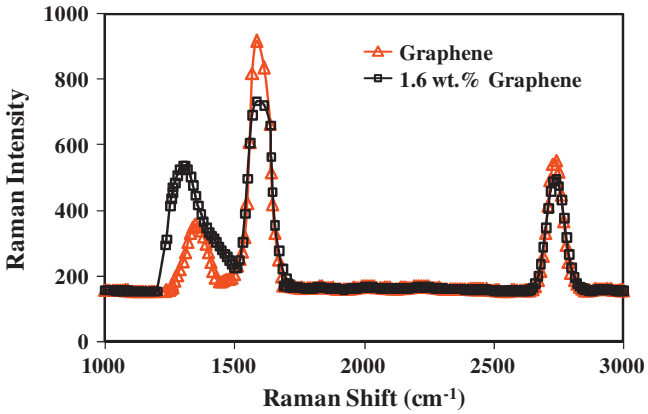

Fig. 5. Raman spectrum of graphene and 1.6 wt% graphene/Sb_2O_3 QDs composites.

also provide the direct evidence of the interaction between graphene and Sb_2O_3 QDs. But in the presence of high density of vacancies and dangling bonds, XPS analysis suffered from adsorbed atmospheric oxygen. As adsorbed atmospheric oxygen have high tendency to adsorb on high vacancies materials. At the same time, Raman spectroscopy effectively shows the interaction between graphene and Sb_2O_3 in the presence of adsorbed atmospheric oxygen through change in D band [13].

Fig. 6 shows the selectivity response of as-fabricated chemiresistors towards CO_2 and LPG for 50 ppm. The composites are highly

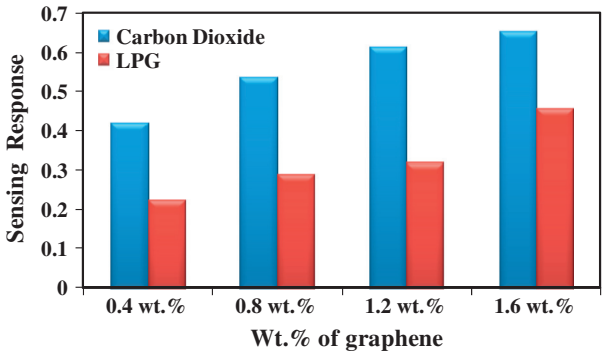

Fig. 6. Comparative gas sensing responses of chemiresistors towards CO_2 and LPG for 50 ppm at room temperature.

selective towards the CO_2 as compare to liquid petroleum gas (LPG). It is directly notable that 1.6 wt% graphene/Sb_2O_3 QDs composites chemiresistor is highly selective than other chemiresistors.

As the composites samples more selective towards the CO_2, sensing capability is tested by recording chemiresistor resistance change when the chemiresistor is exposed to CO_2 with different concentrations. Fig. 7 shows the sensing response to various CO_2 concentrations at room temperature. The sensing response of the chemiresistors to CO_2 is roughly linear, as shown Fig. 7 and it is also scrutinized that sensing response increases with an increase in wt% of graphene.

Fig. 8 shows the operating temperature dependence of the sensing response to 30 ppm CO_2. In the measured temperature range, the responses to 30 ppm CO_2 increases at first, undergoes a maximum, and finally drops. The response value start to drop from particular temperature, this may be due to desorption of atmospheric oxygen ions from sensing surface due to thermal vibrations [14]. The highest value of the sensing response was found at 423 K. Thus, for CO_2 gas detection, the operating temperature of the chemiresistor can be 423 K. This value of operating temperature clearly shows that prepared chemiresistor was operable at low temperature. As the chemiresistor operable at low temperature, gas sensing set up achieve this temperature value by using low electricity. This shows that operation of chemiresistor at low temperature is results in low power consumption. This significantly reduced the operation cost.

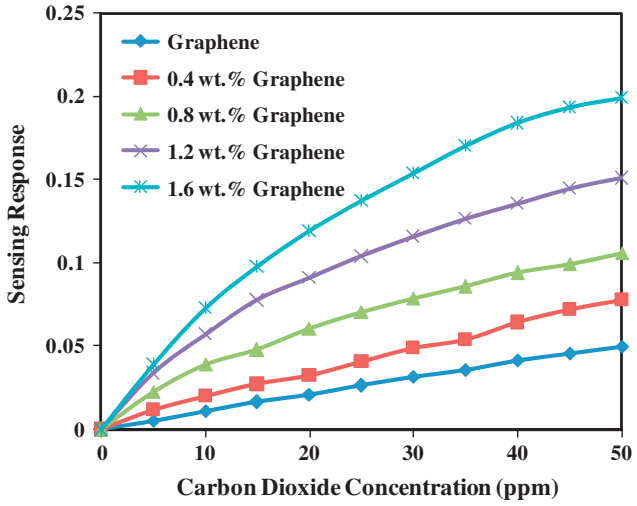

Fig. 7. The variation of sensing response of chemiresistors with the concentration of CO_2 at room temperature.

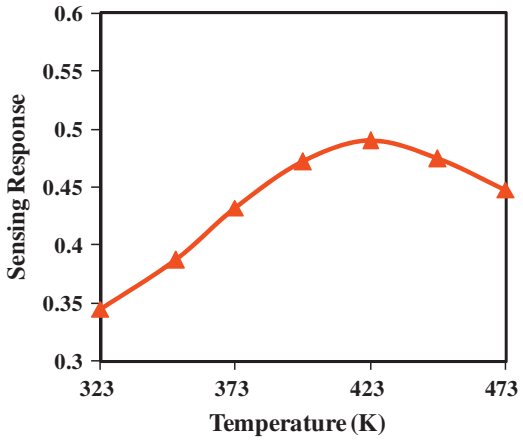

Fig. 8. Chemiresistor response as a function of operating temperature to 30 ppm CO_2.

In order to explain primary mechanism for CO_2 detection, we suggest that the oxygen adsorbed on the surface of samples may be involved in the sensing process of CO_2. The interaction between adsorbed atmospheric oxygen and sensing surface are shown below [15].

$$O_2(gas) \rightarrow O_2(ads)$$

$$O_2(ads) + e^- \rightarrow O_2^-(ads)$$

$$O_2^-(ads) + e^- \rightarrow 2O^-(ads)$$

As gas sensing response depends upon defects density through the oxygen vacancies, which can act as adsorption sites for atmospheric oxygen. Therefore, more number of defects adsorbed more atmospheric oxygen. CO_2 may initially adsorb on pre-adsorbed oxygen and form surface carbonate. This surface carbonates as shown in Fig. 9(a) inject certain electrons from samples, leading an increase in resistance. This shows that formation of surface carbonates was responsible for the CO_2 detection through resistance change.

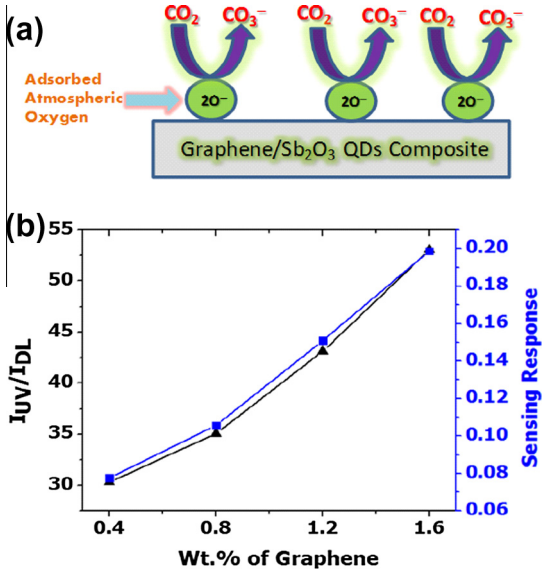

Fig. 9. (a) Plausible sensing mechanism for CO_2 detection. (b) The variation of defects density (I_{UV}/I_{DL}) ratio and CO_2 sensing response with the wt% of graphene.

As the sensing response depends upon defects density, fluorescence measurement becomes crucial. The emission spectrum of composites was used to estimate defects density using intensities ratio of the ultraviolet (I_{UV}) to visible deep levels (I_{DL}) [16]. The oxygen vacancies are the most probable point defects, which increase the probability of adsorption of oxygen on the sensing surface [17]. The variation of I_{UV}/I_{DL} ratio and CO_2 sensing response with the wt% of graphene is shown in Fig. 9(b). From the plots, it is scrutinized that sensing response increases with defects density that is (I_{UV}/I_{DL}) ratio linearly as a function of wt% graphene. As wt% of graphene increases, more and more graphene sheets comes in contact with Sb_2O_3 QDs and damaged. This may be due to Sb_2O_3 QDs act as active sensing sites by damaging to the graphene sheets, which may generates vacancies or dangling bonds on graphene surface and subsequently, enhance defects density [18]. This result is consistent well with the observation made by previous reports [17,19]. Also, this result well supported by Raman spectroscopy. Therefore, 1.6 wt% graphene/Sb_2O_3 QDs shows high selectivity and sensing response towards the CO_2.

Fig. 10 shows stability response of the 1.6 wt% graphene/Sb_2O_3 chemiresistor at room temperature to 50 ppm concentration of CO_2. In order to check the stability of chemiresistor, its response was measured for 30 days, at an interval of 5 days. The chemiresistor has almost constant sensing response. This indicates that stability of chemiresistor is good against CO_2.

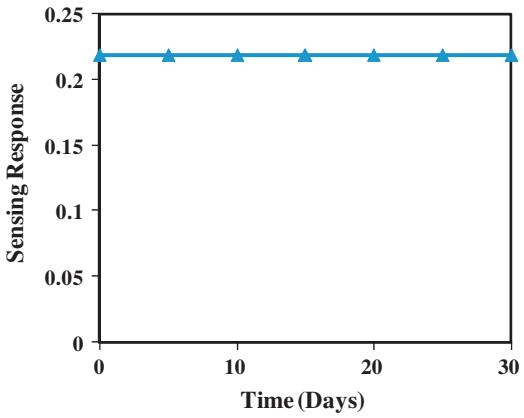

Fig. 10. Stability characteristics of 1.6 wt% graphene/Sb_2O_3 QDs chemiresistor to 50 ppm CO_2.

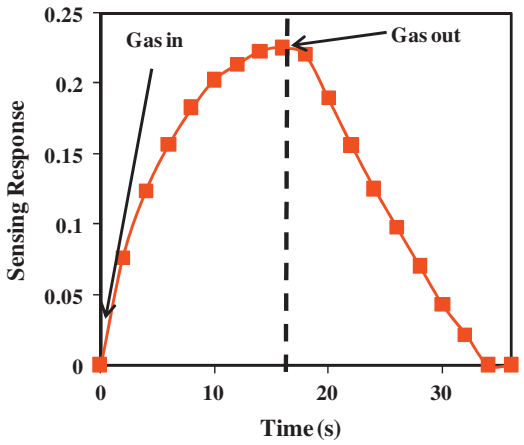

Fig. 11. Transient response of 1.6 wt% graphene/Sb_2O_3 QDs chemiresistor to 50 ppm CO_2.

The transient response characteristic of 1.6 wt% graphene/Sb_2O_3 QDs composite chemiresistor to 50 ppm CO_2 was studied at room temperature and displayed in Fig. 11. In this measurement, gas introduces in the chamber and resistance of chemiresistor was measured in air and in presence of gas. The chemiresistor shows fast response time towards the CO_2 of the order 16 s. For measuring the recovery time, chemiresistor was uncovered to air. The chemiresistor achieve fast recovery in 22 s.

4. Conclusions

In summary, the present work shows that CO_2 sensing response increases with an increase in wt% of graphene. The possible sensing mechanism for CO_2 detection is discussed by using defect chemistry. The present study shows that sensing response is defect density based phenomenon, which effectively analyzed by fluorescence spectroscopy.

Acknowledgements

The authors of present work are very much thankful to Head, Department of Physics Sant Gadge Baba Amravati University, Amravati for providing necessary facilities. One of the authors, K.R. Nemade is very much thankful to Sant Gadge Baba Amravati University, Amravati for awarding Late M N Kale scholarship for the Ph.D. work.

References

[1] C.E. Booth, D.G. McDonald, P.J. Walsh, Mar. Biol. Lett. 5 (1984) 347–358.
[2] K.R. Nemade, S.A. Waghuley, Solid State Sci. 22 (2013) 27–32.
[3] K.R. Nemade, S.A. Waghuley, AIP Conf. Proc. 1536 (2013) 1258–1259.
[4] K.R. Nemade, S.A. Waghuley, Int. J. Mod. Phys.: Conf. Ser. 22 (2013) 380–384.
[5] R. Pasricha, S. Gupta, A.K. Srivastava, Small 5 (2009) 2253–2259.
[6] J.B. Liu, S.H. Fu, B. Yuan, Y.L. Li, Z.X. Deng, J. Am. Chem. Soc. 7279 (2010) 132–153.
[7] J. Li, C.Y. Liu, Eur. J. Inorg. Chem. 8 (2010) 1244–1248.
[8] K.R. Nemade, S.A. Waghuley, J. Elec. Mater. 42 (2013) 2857–2866.
[9] B.C. Yadav, S. Singh, A. Yadav, Appl. Surf. Sci. 257 (2011) 1960–1966.
[10] Y. Wu, B. Wang, Y. Ma, Y. Huang, N. Li, F. Zhang, Y. Chen, Nano. Res. 3 (2010) 661–669.
[11] N.K. Memon, S.D. Tse, J.F. Al-Sharab, H. Yamaguchi, A.B. Goncalves, B.H. Kear, Y. Jaluria, E.Y. Andrei, M. Chhowalla, Carbon 49 (2011) 5064–5070.
[12] K.R. Nemade, S.A. Waghuley, Res. Phys. 3 (2013) 52–54.
[13] L. Meng, S. Park, Bull. Korean Chem. Soc. 33 (2012) 209–214.
[14] K.R. Nemade, S.A. Waghuley, J Chin. Adv. Mater. Soc. 1 (2013) 219–228.
[15] K. Fan, H. Qin, L. Wang, L. Ju, J. Hu, Sens. Actuators, B 177 (2013) 265–269.
[16] O. Lupan, V.V. Ursaki, G. Chai, L. Chow, G.A. Emelchenko, I.M. Tiginyanu, A.N. Gruzintsev, A.N. Redkin, Sens. Actuators, B 144 (2010) 56–66.
[17] S. Pati, S.B. Majumder, P. Banerji, J. Alloys Comp. 541 (2012) 376–379.
[18] Z. Ni, Y. Wang, T. Yu, Z. Shen, Nano. Res. 1 (2008) 273–291.
[19] M.W. Ahn, K.S. Park, J.H. Heo, J.G. Park, D.W. Kim, K.J. Choi, J.H. Lee, S.H. Hong, Appl. Phys. Lett. 93 (2008) 263103–263106.